Available online at www.sciencedirect.com

ScienceDirect

Geochimica et Cosmochimica Acta 257 (2019) 80–95

Geochimica et Cosmochimica Acta

www.elsevier.com/locate/gca

Advected glacial seawater preserved in the subsurface of the Maldives carbonate edifice

Clara L. Blättler [a,b,*], John A. Higgins [b], Peter K. Swart [c]

[a] Department of the Geophysical Sciences, University of Chicago, Chicago, IL 60637, USA
[b] Department of Geosciences, Princeton University, Princeton, NJ 08544, USA
[c] Department of Marine Geosciences, Rosenstiel School of Marine and Atmospheric Science, University of Miami, Miami, FL 33149, USA

Received 2 March 2019; accepted in revised form 29 April 2019; available online 9 May 2019

Abstract

Analysis of both conservative and reactive geochemical tracers in pore fluids extracted from sediment cores from the Maldives Inner Sea reveal extensive interstitial water masses whose origins lie in glacial intermediate water advected laterally through the Maldives carbonate edifice. These drillcores, recovered during Expedition 359 of the International Ocean Discovery Program, penetrate late Oligocene to Recent sediments including carbonate platform, slope, pelagic, and drift facies. Combined shipboard and shore-based analyses of the pore fluids show linearly co-varying changes in the concentration of chloride and $\delta^{18}O$ and δD values of 25 mM, 1.2‰, and 9‰, respectively. Additionally, pore fluid strontium concentrations and calcium isotope ratios are strongly anti-correlated with each other. Multiple reversals in these geochemical properties with depth indicate the existence of several distinct interstitial water masses. These variations are interpreted as representing the different ages and reactive histories of young (Pleistocene and Holocene) waters advecting through the much older sedimentary formations. In particular, the elevated chloride concentrations and water isotope ratios suggest that seawater from the Last Glacial Maximum is preserved in the subsurface, where it occupies over 400 m of the sediment column within Mid- to Late Miocene sediments. These pore fluids constrain the properties of an intermediate depth glacial water mass that had higher salinity and $\delta^{18}O$ and δD values than the average glacial ocean. This system represents a unique archive yielding the most direct observations of glacial seawater to date, as well as a demonstration of the long-lasting potential for water-rock interaction in carbonate platform systems.

1. INTRODUCTION

Understanding the composition of seawater during the Last Glacial Maximum (LGM) has long been a target of paleoceanographic investigation. The oxygen isotopic composition ($\delta^{18}O$ values) of LGM seawater shapes the interpretation of canonical carbonate $\delta^{18}O$ records (Emiliani, 1955; Shackleton, 1977), allowing the extraction of temperature effects from these records. Additionally, resolving glacial chlorinity, as a proxy for salinity, permits density reconstructions of LGM water masses, providing insights into glacial ocean circulation (Adkins et al., 2002). One of the most direct approaches to this information comes from pelagic sedimentary pore fluid profiles where diffusion from the overlying bottom waters has preserved remnant properties of LGM seawater within the upper 10s of meters below the seafloor (McDuff, 1985). By modeling these pore fluid systems, assuming the relative history of the bottom water properties is known, the peak glacial salinity and $\delta^{18}O$ values of local water masses have been reconstructed (Schrag et al., 1996, 2002; Adkins et al., 2002). However, recent

* Corresponding author at: Department of the Geophysical Sciences, University of Chicago, Chicago, IL 60637, USA.
E-mail address: cblattler@uchicago.edu (C.L. Blättler).

https://doi.org/10.1016/j.gca.2019.04.030
0016-7037/

work has shown that the uncertainty on these reconstructions is sufficiently large to limit the potential for paleoceanographic interpretations of LGM circulation (Miller et al., 2015; Wunsch, 2016b,a).

The uncertainties in estimating LGM water mass properties from this approach stem directly from the nature of the archive: diffusion has attenuated the LGM maxima in $\delta^{18}O$ values and chloride concentrations by approximately half. As a result, estimates for endmember LGM seawater are sensitive to the modeling of the diffusive system, in particular to the estimated effective diffusivity and bottom water history (Adkins and Schrag, 2003; Miller et al., 2015; Wunsch, 2016b). Without assuming knowledge about the exact magnitude and timing of variations in sea level and/or $\delta^{18}O$ values, which anyhow reflect global mean conditions and not necessarily the regional properties of interest, the estimates of chloride and $\delta^{18}O$ values are not precise enough to test hypotheses about the distribution of salinity variations in the glacial ocean and their role in driving deep water circulation (Miller et al., 2015; Wunsch, 2016b,a). This method is also limited to deep-sea sites where pore fluid profiles are most likely to be dominated by diffusion and minor advection in the vertical direction, leaving gaps in understanding the LGM history of intermediate depth water masses.

This study documents an alternative geological reservoir that appears to preserve the unattenuated oxygen isotope and chlorinity properties of an intermediate depth LGM water mass in the Indian Ocean. Expedition 359 of the International Ocean Discovery Program (IODP) drilled within the Maldives carbonate edifice, recovering over 3 km of carbonate-rich sediment cores from which pore fluids were extracted. These pore fluids reveal extensive subsurface water masses with distinct properties that include a relatively direct remnant of glacial seawater, largely unaffected by diffusion or dispersion. The variation across profiles of both conservative (chloride concentrations, oxygen isotope ratios, hydrogen isotope ratios) and reactive (calcium isotope ratios, strontium concentrations) tracers at different drill sites suggests a complex structure of flow patterns and water masses of different ages within the sediments of the Maldives. This inferred flow regime shares some similarities but also notable differences compared to other carbonate systems where subsurface flow has been studied, e.g. the Bahamas and Florida Plateau (Kohout et al., 1977; Simms, 1984; Whitaker and Smart, 1990). The storage of advected glacial seawater within the interstitial fluids of the Maldives appears to be a unique finding at present, and investigation of this system provides a test for hypotheses about the role of salinity differences in glacial thermohaline circulation (Adkins et al., 2002). In addition, the complexity of inferred flow and water-rock interaction within the sedimentary formations highlights the challenges of understanding the fidelity of geochemical proxies in analogous depositional environments.

2. METHODS

2.1. Sampling

In 2015, IODP Expedition 359 drilled at eight sites in the inter-atoll channels and Inner Sea of the Maldives archipelago (Fig. 1). Recovered sediments include Miocene to Recent drift deposits overlying the reef, slope, and basinal sediments of a drowned carbonate platform (Betzler et al., 2017, 2018). The aggradation, progradation, and eventual demise of this segment of the carbonate platform system are readily identifiable in seismic reflection data (Fig. 2); the platform drowning has been biostratigraphically dated to 13.0–12.9 Ma (Betzler et al., 2016, 2018). In this study, pore fluid samples were analyzed from three sites (Sites U1465, U1466, and U1468) on an east–west transect lying north of Goidhoo Atoll that penetrate the drowned platform and slope and overlying proximal drifts, as well as two sites (Sites U1471 and U1467) farther east from both the modern and Miocene platform systems, within the Inner Sea, that consist largely of hemi-pelagic drift sediments (Fig. 1, Table 1). Samples of the overlying seawater recovered in the first piston core that penetrated the sediments at each site were also collected, filtered, and stored. Bottom water temperatures measured at Sites U1465, U1466, U1467, and U1471 range from 12–15 °C (Betzler et al., 2017).

Standard IODP methods for pore fluid extraction were used at all sites. Whole-round core intervals 5 to 15 cm long were cut and processed immediately after recovering cores on deck. The exterior of the core was trimmed to remove potential contamination from drilling fluids. The sample was then placed in a titanium sleeve and squeezed under a hydraulic press. Fluids were filtered through a 0.45 μm polyethersulfone membrane filter into an acid- and water-cleaned syringe and transferred to storage vials. The depth given for each sample represents the top of the core interval taken.

At Sites U1466 and U1467, additional pore fluid samples were obtained at higher resolution in the upper 40 m of the sediment core using Rhizon samplers. These samples were extracted a few hours after cores arrived on board, in contrast to those from traditional squeezing methods. Holes were drilled in the core liner to allow the insertion of the 2.5 mm-diameter Rhizon tubes towards the center of the core. The tubes are constructed with a 0.15 μm pore size hydrophilic membrane of polyvinylpyrrolidine and polyethersulfone and attach to a syringe. A vacuum was created in the syringe to extract fluids, which were then transferred to storage vials.

Aliquots of pore fluid for oxygen and hydrogen isotope analyses were placed in 2 mL glass ampules and sealed with a torch. Additional aliquots were acidified with nitric acid for trace element analysis by inductively coupled plasma atomic emission spectroscopy (ICP-AES). The limit for collecting pore fluids at each site was determined by decreased porosity and increased lithification with depth.

2.2. Shipboard data collection

The concentrations of various species in the pore fluids were analyzed using standard shipboard methods on the R/V *JOIDES Resolution* (additional details in Gieskes et al., 1991; Murray et al., 2000; Betzler et al., 2017). Chloride (Cl^-) concentrations were measured by titration with silver nitrate using a Metrohm autotitrator, calibrated

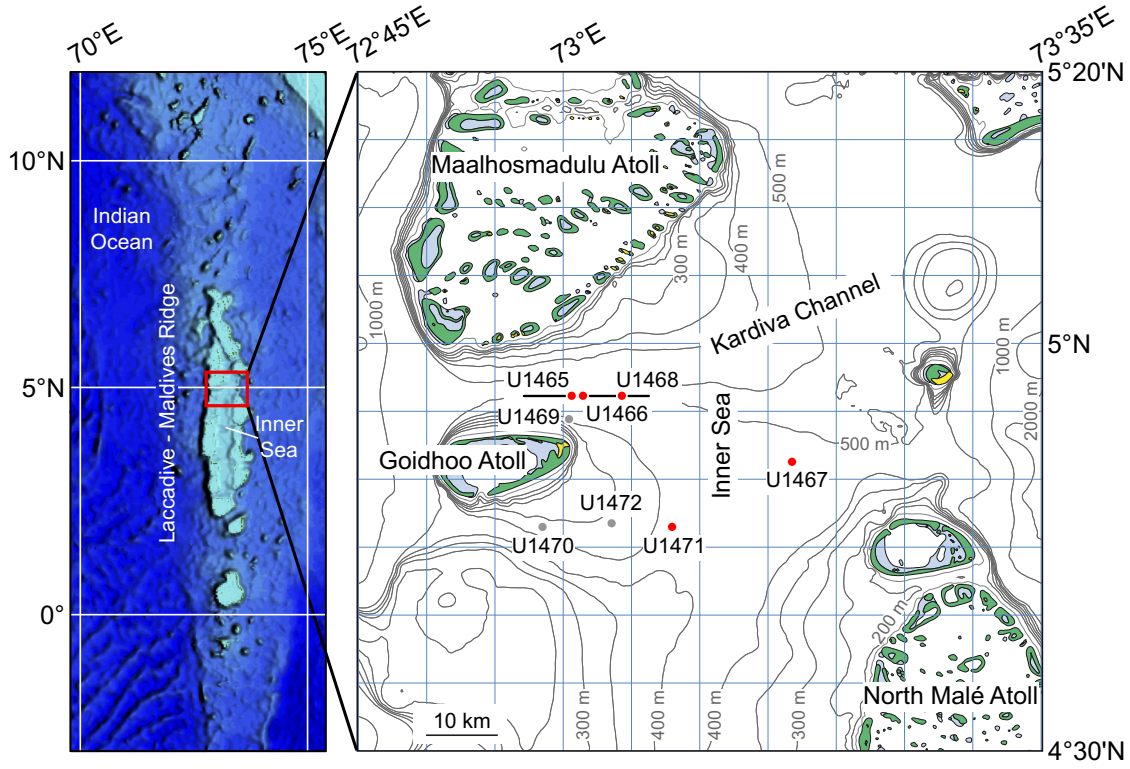

Fig. 1. Regional map showing location of IODP Expedition 359 drill sites, with red markers indicating sites analyzed in this study. Red box indicates area of enlarged map at right. Horizontal line through Sites U1465, U1466, and U1468 represents the seismic transect shown in Fig. 2. Modified from Betzler et al. (2017). (For interpretation of the references to color in this figure legend, the reader is referred to the web version of this article.).

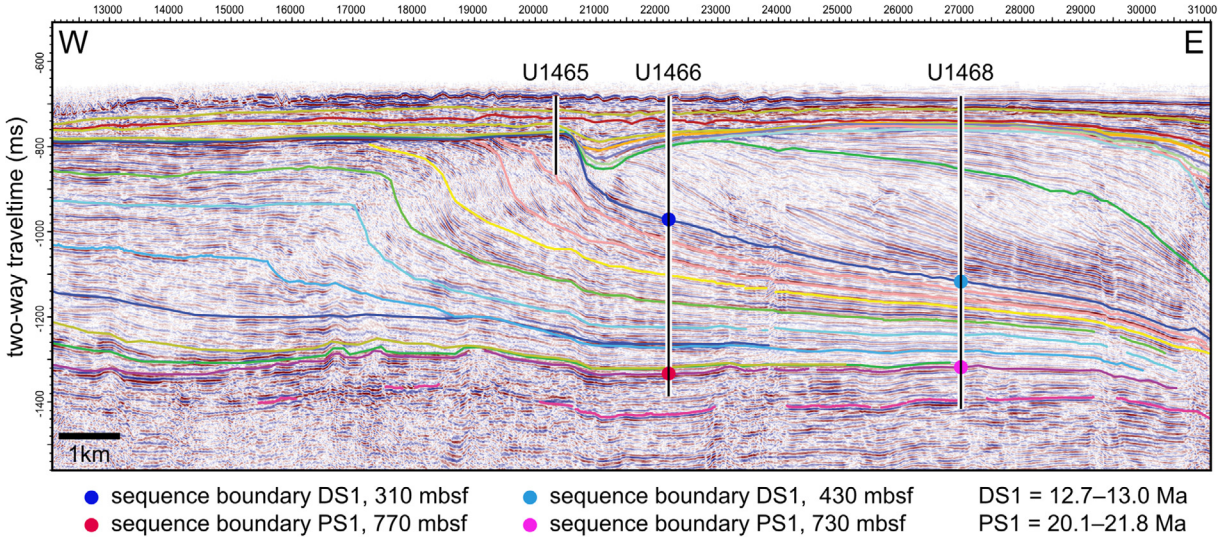

Fig. 2. Multi-channel seismic reflection data from an east-west transect intersecting Sites U1465, U1466, and U1468 (with vertical exaggeration). Colored lines show interpreted sequence boundaries with depths and ages from Betzler et al. (2018). (For interpretation of the references to color in this figure legend, the reader is referred to the web version of this article.).

against repeated titrations of IAPSO standard seawater. This method titrates chloride as well as other halides, although the contribution of other halide components in marine systems can be neglected (less than 0.2% of the chloride concentration). Precision was better than 0.5%.

The concentrations of strontium, along with other trace elements not discussed here, were obtained by shipboard ICP-AES. Samples were acidified and diluted with 2% nitric acid, and yttrium was added as an internal standard. Strontium concentrations were determined using the wavelength

Table 1
Information about drill sites (data from Betzler et al., 2017).

Site	U1465	U1466	U1468	U1471	U1467
Latitude	4°55.99′N	4°55.99′N	4°55.98′N	4°45.98′N	4°51.03′N
Longitude	73°0.68′E	73°1.69′E	73°4.28′E	73°8.11′E	73°17.02′E
Water depth	513 m	518 m	521 m	419 m	487 m
Approx. distance from western Maldives margin	21 km	23 km	28 km	35 km	52 km
Deepest pore fluid collected	69 mbsf	309 mbsf[a]	838 mbsf	528 mbsf[b]	701 mbsf

[a] One additional sample at 510 mbsf.
[b] Two additional samples at 675 and 694 mbsf.

421.552 nm, calibrated against a dilution series of IAPSO standard seawater.

2.3. Shore-based isotopic analyses

Isotopic ratios of oxygen, hydrogen, and calcium in the pore fluids were obtained in shore-based laboratories following the expedition. Oxygen and hydrogen isotope ratios of water ($\delta^{18}O$ and δD values) were measured using a Picarro L2140-*i* Cavity Ring-Down Spectrometer (CRDS). Four standard waters, calibrated to the SMOW–GISP–SLAP scale (Standard Mean Ocean Water, Greenland Ice Sheet Precipitation, and Standard Light Antarctic Precipitation), were analyzed at the beginning and end of a block of 19 samples. Each sample or standard was injected six times into the Picarro A0211 vaporizer unit, held at 110° C for the duration of the sample run, using N_2 as the carrier gas and 1.8 µL per injection. Salt from the sample was retained within a fine mesh basket positioned below the septum in the injection port, which was removed and cleaned between each run of 19 samples and 8 standards. The first two injections from each sample are routinely discarded to eliminate any memory between samples. Samples processed between the initial and final standards are corrected for any drift in the instrument, although this is usually minimal. The data are reported relative to VSMOW using the conventional notation and have an average standard deviation of <0.04‰ for $\delta^{18}O$ and <0.1‰ for δD, where the error represents the mean standard deviation of all injections used to calculate the mean values of standards and samples.

For calcium isotope analysis, acidified pore fluid samples (residues from shipboard alkalinity titration by hydrochloric acid) were diluted to approximately 30 ppm calcium for ion chromatography with an automated Thermo-Dionex ICS-5000+. Chromatographic separation of calcium followed previously published methods (Blättler et al., 2015), using a CS-16 5 × 250 mm cation-exchange column with methanesulfonic acid as an eluent. Elution times for pore fluid samples were approximately 50 min per sample, including column washing back to baseline levels, which achieves clean separation of ions and a blank of <5 ng calcium (Fig. 3). An in-line conductivity detector provided real-time quality control for the ion chromatography. The purified solutions of calcium were then dried down, dissolved in 200 µL of distilled concentrated nitric acid, dried down again, and then finally redissolved in 2% nitric acid to a concentration of 2 ppm calcium (±5%). Calcium isotope standards of matching concentration were prepared, and sample-standard bracketing was used to measure isotopic ratios on a Thermo Neptune Plus multi-collector inductively coupled plasma mass spectrometer (MC-ICP-MS). A desolvating sample introduction system (ESI Apex-IR) was used to minimize hydride interferences. Corrections for isobaric strontium interferences were performed based on the intensity of $^{87}Sr^{2+}$; polyatomic interferences (e.g. $^{40}ArHH^{+}$) were avoided with sufficient mass resolution. Based on the intensities of ^{44}Ca, ^{43}Ca, and ^{42}Ca, which show the expected mass dependence (Fig. 4), $\delta^{44/42}Ca$ ratios were calculated and converted to $\delta^{44/40}Ca$ values following kinetic mass fractionation laws (Young et al., 2002) assuming no radiogenic ^{40}Ca excess (Caro et al., 2010). External precision on $\delta^{44/40}Ca$ values is ±0.14‰ (2σ), derived from the long-term reproducibility of the carbonate standard SRM-915b treated as an unknown sample (n = 199). The $\delta^{44/40}Ca$ value obtained for SRM-915b is −1.15‰, which is indistinguishable from published values (Heuser and Eisenhauer, 2008; Jacobson et al., 2015).

3. RESULTS

The new analyses presented in this paper are combined with previously reported concentration data (Betzler et al., 2017) in Figs. 5–7, with the sites ordered by their east-west position. The structure of the profiles of chloride, $\delta^{18}O$, and δD values are broadly similar to each other, but very different across the sites (Figs. 5 and 6). Similarly, $\delta^{44/40}Ca$ values and strontium concentrations share many

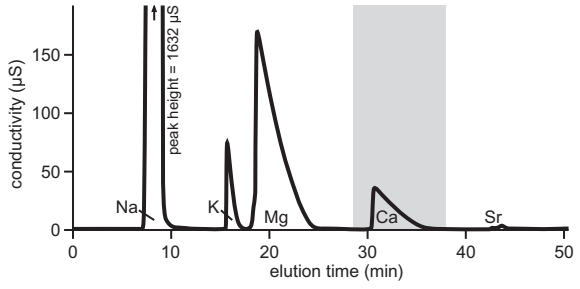

Fig. 3. Chromatograph of a pore fluid sample (U1466A-5H-4-140-150-IW) showing the clean separation of calcium from other major cations in a seawater-like matrix. The gray window indicates the collection interval.

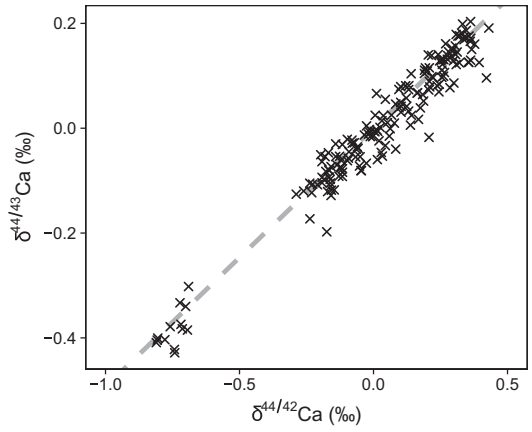

Fig. 4. Raw delta values (not normalized to an external standard) reflecting the measured mass fractionation relationship among ^{44}Ca, ^{43}Ca, and ^{42}Ca. Dashed line shows the theoretical kinetic mass fractionation law with $\beta = 2.027$ for $^{44/42}R$ and $^{44/43}R$ (Young et al., 2002).

features of their pore fluid profiles, yet differ somewhat across sites (Fig. 7). The overlying seawater, sampled at all sites, has average chloride, $\delta^{18}O$, δD, strontium, and $\delta^{44/40}Ca$ values of 560 mM, 0.3‰, 2.7‰, 88 μM, and −0.05‰, respectively.

At Site U1465, pore fluid samples were only collected from the sheeted drift sediments overlying the drowned Miocene platform. Over this depth interval, all measured concentrations and isotopic ratios remain essentially invariant and equal to values measured in the overlying seawater.

Site U1466 yielded pore fluids from the sediment-water interface through the mid-Miocene (Serravallian) drift deposits. Chloride concentrations increase from 0 to 68 mbsf, below which they remain steady around 585 mM. The increase is very gradual between 0 and 42 mbsf before climbing steeply between 42 and 68 mbsf. This pattern is closely mimicked in the profiles of $\delta^{18}O$ and δD values, which increase from bottom water values of 0.4‰ and 3‰, respectively, to peaks of 1.6‰ and 12‰ around 100 mbsf, including rapid increases between 42 and 68 mbsf. Below these peaks, $\delta^{18}O$ and δD values decrease slightly to 1.2‰ and 10‰, respectively, at greater depths. Calcium isotope ratios and strontium concentrations show anti-correlated behavior, with $\delta^{44/40}Ca$ values decreasing from 0 to −0.5‰ over the upper 30 mbsf of the profile before leveling off between 30 and 125 mbsf and then decreasing gradually to −0.9‰ at 309 mbsf. Strontium concentrations increase from 90 to 150 μM over the upper 30 mbsf before leveling off until 110 mbsf, below which they rise quickly to approximately 400 μM at 200 mbsf and then more gradually to above 460 μM in the deepest pore fluids sampled at this site.

Pore fluid profiles from Site U1468, where the deepest pore fluids were recovered, share many similar features to those from Site U1466, while revealing unexpected trends at greater depths. The profile extends through the mid-Miocene drift deposits into the early to mid-Miocene platform slope sediments. Chloride and $\delta^{18}O$ and δD values rise over the upper 70 mbsf to reach maxima of 585 mM, 1.4‰, and 13‰, respectively, between 70 and 130 mbsf. Below these peaks, chloride decreases gradually to 570 mM by 800 mbsf; $\delta^{18}O$ and δD values decrease to 0.7‰ and 6‰ over the same interval, with a disturbance to this smooth decrease around 410 mbsf. Calcium isotope ratios and strontium concentrations are again roughly anti-correlated, although they diverge from this relationship at certain intervals. In the upper 60 mbsf, $\delta^{44/40}Ca$ values take

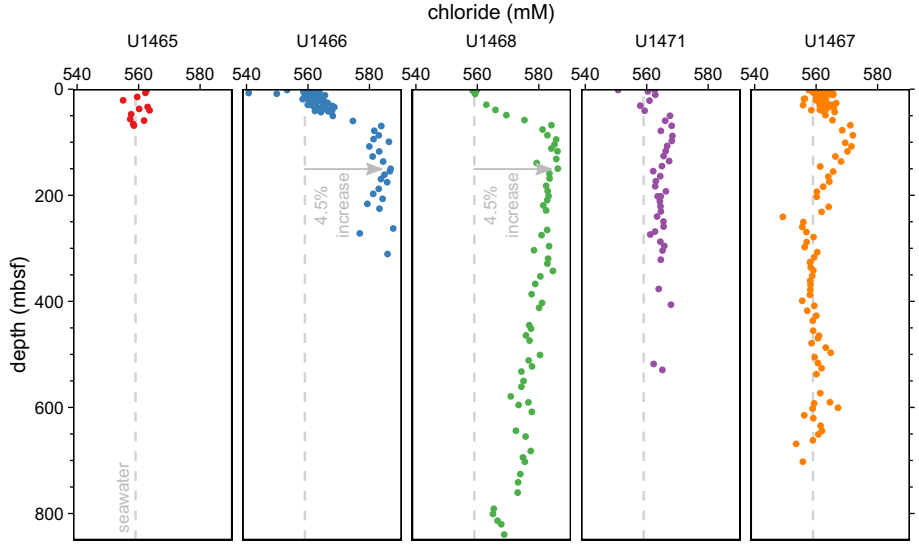

Fig. 5. Profiles of pore fluid chloride concentrations at Sites U1465, U1466, U1468, U1471, and U1467 (shipboard data from Betzler et al., 2017). The higher sampling density in the upper 40 mbsf at Sites U1466 and U1467 reflects the use of Rhizon samplers in those intervals in addition to traditional squeezing methods for pore fluid extraction. Arrows show the magnitude of a 4.5% increase in chloride over the concentration in the overlying seawater.

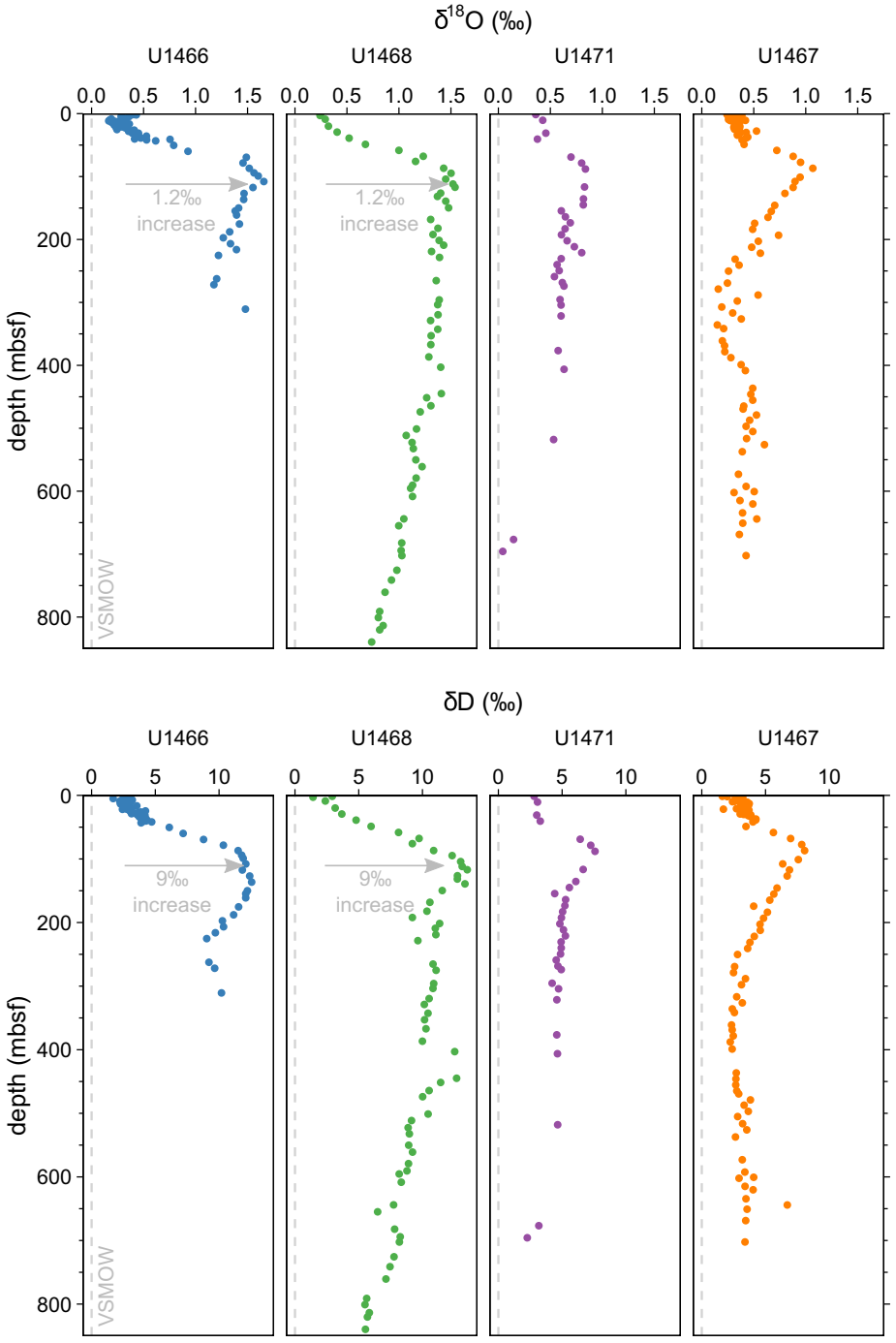

Fig. 6. Profiles of pore fluid water isotope ratios ($\delta^{18}O$ and δD values, relative to VSMOW) at Sites U1466, U1468, U1471, and U1467. Arrows show the magnitude of a 1.2‰ increase in $\delta^{18}O$ values and a 9‰ increase in δD values over the isotopic ratios in the overlying seawater.

a turn towards −0.5‰ before rebounding to −0.1‰. Strontium concentrations instead remain level at 120 μM, slightly above bottom water concentrations. From 200–500 mbsf, $\delta^{44/40}Ca$ values are steady around −0.9‰ and strontium concentrations plateau around 430 μM, following a very rapid increase in concentration at approximately 170 mbsf. Below this plateau, both properties return towards but do not quite attain values seen in the overlying seawater, with $\delta^{44/40}Ca$ values reaching −0.4‰ and strontium concentrations 180 μM at 838 mbsf.

Site U1471, the southernmost site, lying 19 km south of the U1465–U1466–U1468 transect, has pore fluid profiles with notably different structure from the three sites described above. In particular, chloride, $\delta^{18}O$, and δD

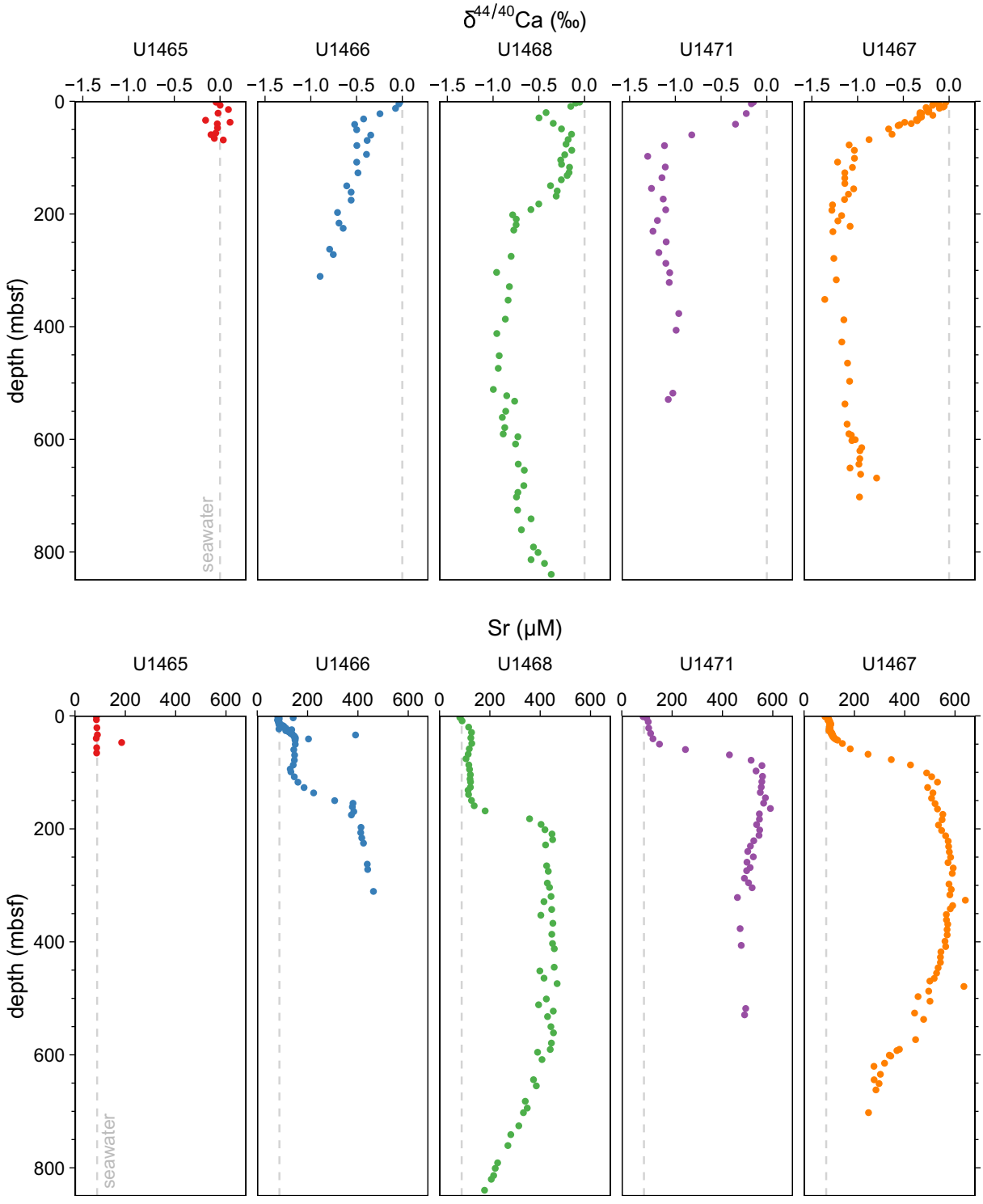

Fig. 7. Profiles of pore fluid calcium isotope ratios ($\delta^{44/40}$Ca values, relative to seawater) and strontium concentrations at Sites U1465, U1466, U1468, U1471, and U1467.

values rise to peaks at approximately 100 mbsf before decreasing to values only slightly higher than those of the bottom water by 180 mbsf and below. The maximum peaks attained for chloride, δ^{18}O, and δD values are 568 mM, 0.8‰, and 7‰, respectively. Calcium isotope ratios decrease over the upper 80 mbsf, below which they remain around −1.1‰. Strontium concentrations increase over the upper 80 mbsf, first gradually and then very rapidly

between 40 and 80 mbsf, reaching maximum concentrations of around 560 μM for the next 100 m before decreasing slightly to approximately 480 μM below 300 mbsf.

The most distant site from the western margin, Site U1467 shares many features in common with Site U1471. Chloride, $\delta^{18}O$, and δD values peak at 570 mM, 1.0‰, and 8‰, respectively, around 80 mbsf. Below these peaks, these pore fluid properties recover more fully to bottom water levels and are largely stable below 250 mbsf. The peaks attained for chloride, $\delta^{18}O$, and δD values are slightly larger than those at Site U1471. Calcium isotope ratios and strontium concentrations are also similar to Site U1471 and anti-correlated with each other, with $\delta^{44/40}Ca$ values decreasing to −1.2‰ over the upper 100 mbsf as strontium concentrations rise to 500 μM. Below 600 mbsf in this core, $\delta^{44/40}Ca$ values increase slightly to around −1.0‰, and strontium concentrations decrease to below 300 μM.

Geochemical crossplots (Fig. 8) demonstrate important relationships between pore fluid properties, as well as similarities and differences among the sites. Chloride and $\delta^{18}O$ values show a clear linear relationship ($r^2 = 0.85$, Fig. 8A), as do δD and $\delta^{18}O$ values ($r^2 = 0.95$, Fig. 8E). A regression line through the $\delta^{18}O$ and δD data for all sites yields a slope of 7.5, close to the slope of 8 expressed in the Global Meteoric Water Line (GMWL), and a δD-intercept of 0.5‰. Calcium isotope ratios and strontium concentrations are generally anti-correlated, but this relationship takes on different slopes at different sites and intervals (Fig. 8B). Sites U1466 and U1468 follow an S-shaped curve in a crossplot, whereas Sites U1471 and U1467 are more similar to a reverse J.

Crossplots of chloride, $\delta^{18}O$, or δD values against either Sr concentrations or $\delta^{44/40}Ca$ values yield complex patterns with multiple endmembers and trends reflected at each site (e.g. Fig. 8C,D). The composition of the overlying bottom water is the only fluid endmember that is shared among Sites U1466, U1468, U1471, and U1467, whose profiles trace out non-overlapping triangles in crossplot space. These relationships highlight the distinct structures of the two pairs of sites, Sites U1466 and U1468 versus Sites U1471 and U1467.

4. INTERPRETATION AND DISCUSSION

4.1. Source of high chlorinity interstitial waters

As a conservative tracer, the elevated chloride concentrations within the pore fluids of the Maldives require different source waters than exist in the surrounding ocean. The excellent correlation between chloride and $\delta^{18}O$ values as well as between $\delta^{18}O$ and δD values (Fig. 8) suggests mixing between two endmembers: modern Indian Ocean seawater and LGM Indian Ocean seawater. Local evaporation and brine formation, which can also generate high chloride, isotopically enriched waters, can be ruled out for several reasons. First, the measured chloride increase, as a conservative proxy for total salinity (Adkins and Schrag, 2003), would not increase the density of surface waters enough to sink and displace waters even to the depth of the seafloor at the drill sites, much less to the subsurface depths where the high chlorinity waters were recovered. In this tropical setting, warm surface waters would need to increase in salinity by over 15% to overcome the density gradient within the Inner Sea, compared to the observed chloride increase of less than 5%. Additionally, the regional geography is not conducive to brine formation compared to other extensive platform systems with documented subsurface brines. The shallow bank-top areas in the Maldives are much smaller, more fragmented, and less restricted than the Great Bahama Bank, for example, and are swept by seasonally reversing monsoonal currents, making it unlikely that these areas could generate the large volume of brine required to fill the thick interval of elevated chloride concentrations observed at Sites U1466 and U1468. Finally, the relationship between $\delta^{18}O$ and δD, with a slope near to that of the GMWL, is consistent with glacial seawater, but not with a local brine, which would be expected to follow a shallower slope to balance the deuterium excess acquired by the tropical water vapor during evaporation. The glacial ocean instead mass balances the strongly depleted polar ice caps and should therefore have a much closer slope to the GMWL, as do the pore fluids in the Maldives. The strong correlations between the three largely conservative tracers also rule out other processes that affect only one but not all of the properties, such as evaporite dissolution or carbonate recrystallization, as being dominant factors affecting the composition of these pore fluids (further discussion of carbonate recrystallization reactions in Section 4.2).

The scale of the glacial seawater signal in the Maldives pore fluids is a key difference between these observations and previous identifications of LGM water mass properties within pelagic pore fluid profiles (e.g. Schrag et al., 1996, 2002; Adkins et al., 2002). Previous work on pelagic sedimentary systems assumed that lateral advection was negligible, and therefore the depth of the LGM peak in chloride concentrations, $\delta^{18}O$, and δD values was controlled by diffusion (and minor advection in the vertical direction, driven by sediment compaction) and expected within a few 10s of meters of the seafloor (Schrag and DePaolo, 1993; Adkins and Schrag, 2003). In contrast, high chloride waters in the Maldives occupy depth intervals hundreds of meters thick (at least 200 m at Site U1466 and over 500 m at Site U1468). Profiles at Sites U1471 and U1467 that look superficially like the diffusive profiles at pelagic sites nevertheless have peak chloride around 100 mbsf, much deeper than expected for the LGM peak with typical sedimentation rates and effective diffusivities (Adkins and Schrag, 2003; Wunsch, 2016b). Instead, the pore fluid profiles in the Maldives appear to be dominated by lateral advection, as has been documented or inferred for other carbonate platform systems (e.g. Kohout, 1967; Kohout et al., 1977; Aharon et al., 1987; Whitaker and Smart, 1990), leading to the preservation of a unique archive of unadulterated endmember glacial seawater.

The magnitude of change in conservative properties of the Maldives pore fluids is also consistent with an LGM origin based on estimates of glacial seawater composition

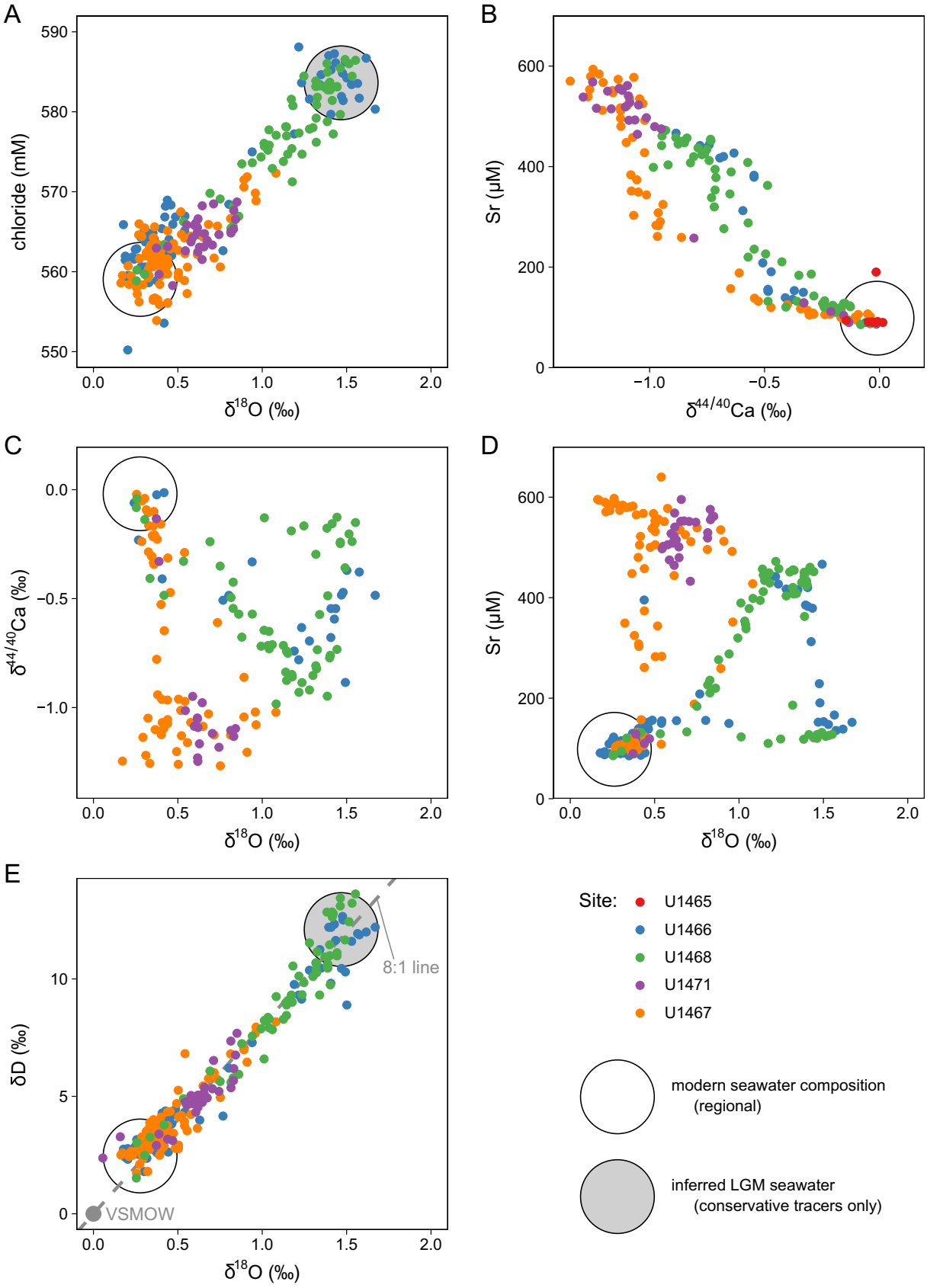

Fig. 8. Crossplots of various geochemical properties measured in IODP Expedition 359 pore fluids.

from diffusion-dominated pore fluid systems (Schrag et al., 1996, 2002; Adkins et al., 2002), despite the inherent uncertainties in that method. Reconstructions of LGM salinity in abyssal water masses from pelagic pore fluid profiles estimate glacial increases of 2.7–6.6% over modern mean ocean salinity (Adkins et al., 2002). (Note that these reconstructions are derived from observed chloride increases of only 1.2–2.8%, the true magnitude of the LGM signal being attenuated by diffusion.) Glacial seawater $\delta^{18}O$ values similarly estimated from pelagic pore fluid profiles yield LGM increases of 0.7–1.4‰, derived from observed pore fluid increases of 0.2–0.7‰ (Schrag et al., 1996, 2002; Adkins et al., 2002). In the few locations where deuterium has also been analyzed, δD values have been observed to follow the behavior of $\delta^{18}O$ values times a factor of eight (Schrag et al., 2002), tracking parallel to the GMWL. Compared to these estimates, the waters preserved in the subsurface of the Maldives fall towards the upper end of these ranges and are therefore consistent with an LGM origin: based on Sites U1466 and U1468, the intermediate depth LGM water mass has increases in chloride of 4.5% (559–584 mM), $\delta^{18}O$ values of 1.2‰ (0.3–1.5‰), and δD values of 9‰ (3–12‰) (Figs. 5 and 6). All these pore fluid estimates reflect the local properties of regional or overlying water masses; for comparison, the global mean change in salinity for a 125 m sea level fall translates to a 3.3% increase (Adkins et al., 2002).

4.2. Reactive history of interstitial waters

Complementing the observations of conservative tracers, measurements of non-conservative species in these pore fluids clarify the reactive history of the interstitial water masses. In particular, carbonate recrystallization reactions, including both calcite recrystallization as well as aragonite-to-calcite neomorphism, have predictable effects on pore fluid calcium isotope ratios and strontium concentrations. Primary carbonate sediments are fractionated from seawater with respect to calcium isotopes ($\delta^{44/40}Ca$ values) by −1.5 to −0.8‰, but diagenetic recrystallization reactions express a much smaller fractionation, leading pore fluid calcium isotope ratios to generally decrease with depth until they equal those of their host sediments (Fantle and DePaolo, 2007; Turchyn and DePaolo, 2011; Higgins et al., 2018). Pore fluid $\delta^{44/40}Ca$ values therefore track progressive recrystallization until isotopic equilibrium with the sediments is reached. Strontium in pore fluids is sensitive to only a subset of these reactions, when strontium-rich primary aragonite (or biogenic calcite) is converted to strontium-poor calcite, releasing strontium into the fluid phase. Together, these two reactive tracers provide additional context on the structure and history of the interstitial water masses, providing a 'reactive age' to complement the glacial/interglacial age derived from the conservative tracers (chloride, $\delta^{18}O$, and δD values).

The general anti-correlated co-variation between calcium isotope ratios and strontium concentrations (Fig. 8B) shows the progression from the seawater endmember (high $\delta^{44/40}Ca$ values, low strontium) to an evolved fluid endmember (low $\delta^{44/40}Ca$ values, high strontium) that has interacted extensively with aragonite-bearing sediments. The upper bound on strontium concentrations is the saturation of the trace mineral celestine ($SrSO_4$), detected within the sediments by X-ray diffraction at Sites U1467, U1468, and U1471 (Betzler et al., 2017), and is dependent on the sulfate concentrations of pore fluids at each site. Of course, the sediments that have interacted with the pore fluids lie upstream along the advective path and may differ in composition from those currently hosting the fluids. Compared to systems dominated by diffusion or transport only in the vertical direction, this represents an additional source of uncertainty in understanding the reactive evolution of both pore fluids and sediments.

Depending on the composition, reactivity, and diagenetic history of the 'upstream' sediments, pore fluids can evolve along different paths with respect to calcium isotope ratios and strontium concentrations, explaining the different slopes expressed across Fig. 8B. For example, shallow negative slopes (substantial variation in calcium isotope ratios with little effect on strontium) can result from recrystallization of calcite rather than aragonite, potentially reflecting previous diagenetic loss of aragonite and flushing away of its strontium content. The neomorphism of pure aragonite with a theoretical composition of $\delta^{44/40}Ca = -1.4‰$ and $Sr = 8000$ ppm would yield a 100 μM increase in strontium over a −0.7‰ change in pore fluid $\delta^{44/40}Ca$ values, which approximately matches certain intervals of the studied pore fluid profiles. Steeper slopes can also arise from mixing between two fluid endmembers, given that the endpoint composition of the evolved pore fluids with respect to each of the reactive tracers is determined independently. Calcium isotopes eventually reach equilibrium with the carbonate sediments, but strontium reaches a maximum concentration determined by saturation of the trace mineral celestine and local sulfate concentrations (Betzler et al., 2017). Since these endpoint values do not scale directly to the extent of aragonite neomorphism, mixing between more and less evolved fluids can generate different relationships between the reactive tracers which translate to different slopes in Fig. 8B. Similarly, different endpoints with respect to pore fluid $\delta^{44/40}Ca$ values for the different sites could arise from equilibration with upstream sediments of various compositions and reactivities that cannot be reconstructed with the samples currently available.

A small amount of net dissolution has occurred at all sites, as indicated by pore fluid calcium concentrations ranging from 10 to 21 mM (Betzler et al., 2017). This amount of dissolution can only explain a fraction of the changes in $\delta^{44/40}Ca$ values and strontium concentrations, which require the reaction (dissolution–reprecipitation) of at least five times as much carbonate sediment with little to no net change in the mass of carbonate or calcium content of the pore fluids. These recrystallization reactions will also affect the oxygen isotope composition of the pore fluid to some degree, although this contribution cannot be quantified precisely because of the lack of borehole temperature constraints for most of the cores (Betzler et al., 2017).

However, the excellent correlations between $\delta^{18}O$ values and both chloride and δD values show that the effect on $\delta^{18}O$ values must be small; additionally, the maximum changes in the reactive tracers can be explained by recrystallization of less than 0.2% of the sedimentary mass (for an initial pure aragonite composition), which would have a negligible effect on pore fluid $\delta^{18}O$ values.

The interplay between conservative and reactive tracers reveals a complex structure of interstitial water masses with different ages and histories. A simple relationship between the glacial/interglacial age of a water mass and its evolution with respect to the reactive tracers ($\delta^{44/40}Ca$ values and strontium concentrations) does not exist, as demonstrated by the complex paths represented in crossplots Fig. 8C and D (also Fig. 9B and C). Site U1468 demonstrates the most complexity in the vertical structure of water masses (Figs. 9 and 10), including from top to bottom: a post-glacial (possibly Holocene) water mass that has experienced minimal exchange with aragonite, although some calcite recrystallization seems to have occurred (0–60 mbsf); a glacial (LGM) water mass that has also not extensively reacted with aragonite (70–170 mbsf); a glacial water mass with evolved $\delta^{44/40}Ca$ values and strontium content, indicating recrystallization with carbonate sediments as well as possible celestine dissolution (200–400 mbsf); a transitional zone with decreasing conservative tracers yet relatively stable reactive tracers (400–600 mbsf); and finally a return to near interglacial water composition with minimal accumulated recrystallization based on the reactive tracers (below 600 mbsf). These deepest pore fluids at Site U1468, with all geochemical properties reversing and returning towards the composition of overlying seawater, raise the possibility that younger Holocene water may be penetrating the sediment column beneath the thick interval of glacial water. The gradual geochemical transitions in the deepest pore fluids suggest that mixing or diffusion may be occurring between these two inferred water masses.

The age of the glacial water mass is not precisely known, although it is assumed to correspond to the LGM by virtue of being the most recent time interval with high chloride, isotopically enriched seawater. However, it cannot be ruled out that the waters could have their origins in older glacial periods; additionally, the glacial water mass can only provide a minimum estimate for peak LGM salinity and $\delta^{18}O$ values. If the evolution of the reactive tracers provides robust relative age information (although this depends on the reactivity of sediments and recrystallization rates), then Sites U1471 and U1467 may preserve last interglacial seawater (Marine Isotope Stage 5), or seawater from an even older interglacial period, below the peaks in conservative tracers. Below 180 and 210 mbsf, respectively, these sites contain modern salinity water masses that have extensively reacted with aragonite-bearing sediments, in contrast to the young (Holocene to Recent) waters near the tops of the cores that have not evolved much with respect to the reactive tracers. Absolute dating of the water masses is not possible because of interaction with the carbonate sediments (interfering with radiocarbon and uranium-series methods, for example) and sampling limitations (oxidation interferes with uranium-series, collected volumes of water limit noble gas methods), so better age constraints cannot be obtained at this time. Lacking additional constraints on the subsurface extent or structure of these water masses, the LGM remains the most parsimonious estimate for the age of the high chloride water masses.

4.3. Possible mechanisms and structure of subsurface fluid flow

The extent of the glacial/interglacial interstitial water masses in the Maldives is not sufficiently well constrained to identify a flow path or mechanism, but some predictions and speculations can be made. The source for the laterally advected waters at Sites U1466 and U1468 is likely to the west, the closest margin of the Maldives edifice, with flow towards the interior (Fig. 11). If the glacial water mass is indeed LGM in age, this geography requires a horizontal flow rate around 1 m/yr; if Holocene water is penetrating underneath the glacial water mass at Site U1468, flow rates at greater depths must be even faster. Although such rates seem high compared to the estimate of 0.11 m/yr for advection on the Bahamas slope (Henderson et al., 1999) and results of certain theoretical simulations (Kaufman, 1994), the Maldives system has important differences in scale and structure that could explain these discrepancies. The estimated flow rate on the Bahamas slope applies to a much shallower advective regime, as well as to a very different sedimentary porosity profile. At Sites U1466 and U1468 in the Maldives, a surprising 45–50% porosity persists to over 800 mbsf (Fig. 12), which may facilitate high rates of lateral advection. The lack of porosity and permeability data throughout the rest of the platform system limits further understanding of the physical properties promoting the proposed flow. However, most model simulations that derive lower flow rates assume both a lower starting porosity and a much stronger decrease in porosity with depth throughout carbonate platforms (Kaufman, 1994). In fact, advection rates on the order of meters per year are within the bounds of other theoretical calculations for platform flow systems (Simms, 1984) as well as estimated rates of seawater penetration into coastal systems (Yechieli et al., 2019) on similar scales to the Maldives. Of course, if the high chloride water masses in the Maldives subsurface originate in older glacial periods, the inferred lateral advection rates would be much reduced.

Among the known mechanisms driving flow in platform systems, the only plausible mechanism matching the scale of the Maldives system is geothermal Kohout convection (Kohout, 1967; Kohout et al., 1977; Simms, 1984; Sanford et al., 1998). The Paleogene volcanic basement, part of the Chagos-Laccadive Ridge system, may be responsible for heating fluids within the approximately 3-km-thick overlying carbonate succession (Duncan and Hargraves, 1990; Aubert and Droxler, 1996). Cool seawater would be drawn into the interior of the platform through the steep-sided (20–30°) margins (Aubert and Droxler, 1996) in response to a horizontal density gradient (Simms, 1984). Unfortunately, attempts to obtain borehole temperature measurements during the expedition were largely

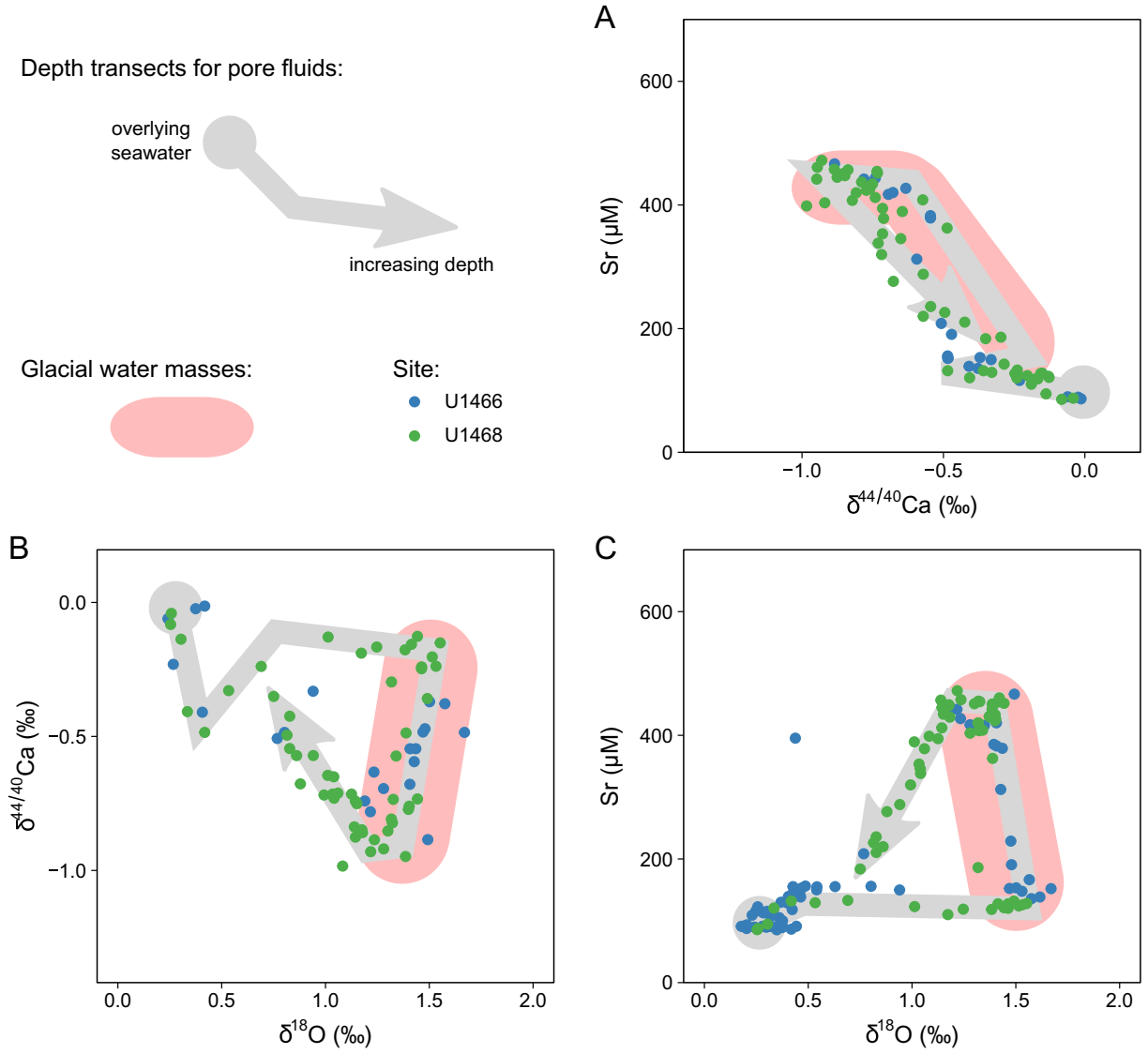

Fig. 9. Crossplots of geochemical properties at Sites U1466 and U1468 only, showing the evolution of pore fluid geochemistry with depth (trajectory of gray arrows) and identifying glacial water masses.

unsuccessful, although the few measurements obtained from shallow depths at Sites U1465, U1466, U1467, and U1471 show lower temperatures than bottom water mudline temperatures and a remarkably low temperature gradient from 0 to 170 mbsf at Site U1471, which are consistent with the proposed circulation (Betzler et al., 2017). Kohout convection, extending well below a kilometer depth, occurs today within the Florida Plateau, with a major difference being the involvement of a large freshwater lens in Florida (Kohout et al., 1977). Large scale circulation in the Great Bahama Bank may reflect a combination of evaporative reflux as well as geothermal Kohout convection, involving brines of much greater salinity than found in the Maldives (Whitaker and Smart, 1990; Caspard et al., 2004). A closer analogy to the Maldives flow system, although on a smaller scale, may be isolated Pacific atolls, whose extensive dolomitization and borehole temperature profiles can be explained by similar deep convective processes (Saller, 1984; Aharon et al., 1987). Compaction-driven flow may be relevant on small scales where the sediments are not extensively lithified, but it is not capable of driving the large-scale horizontal flow inferred for the Maldives. All the drill sites of IODP Expedition 359 are well below the depth of subaerial exposure during Pleistocene glacial sea level falls and would have remained submerged during their recent history.

The outflow of the proposed convective cell may exist within the Inner Sea of the Maldives, where unusual pockmark structures have been observed and interpreted as venting features for gas and fluids (Betzler et al., 2011). These features are sometimes associated with subsurface faults, which may be responsible for changing the permeability structure of the sedimentary succession, disrupting stratigraphic barriers to vertical transport, and providing

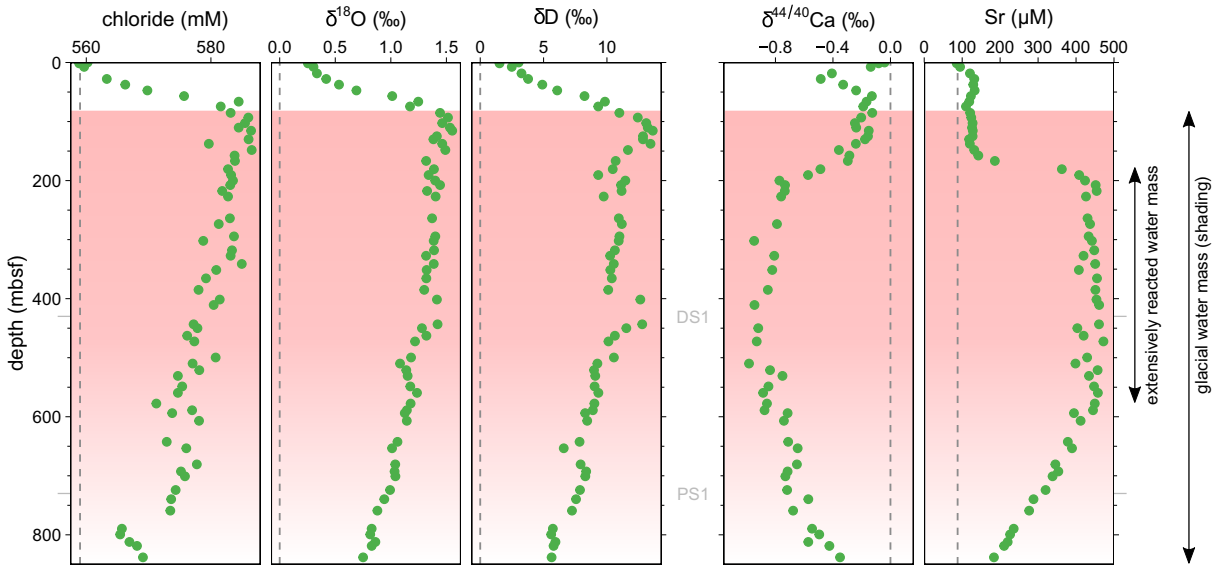

Fig. 10. Profiles of pore fluid geochemical properties at Site U1468. Vertical dashed lines show seawater values (VSMOW for $\delta^{18}O$ and δD values). Shading represents the relative contribution of glacial seawater to the conservative geochemical tracers in the pore fluids; one interval within the glacial water mass is more extensively reacted than waters both above and below. DS1 and PS1 refer to sequence boundaries (see Fig. 2).

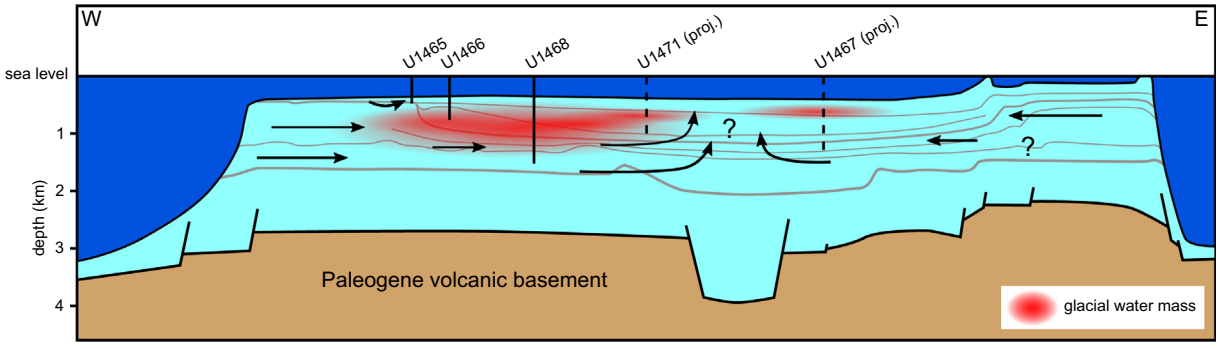

Fig. 11. Cartoon showing speculative flow patterns (black arrows) across a 2D cross section of the Maldives edifice (platform structure modified from Betzler et al. (2018). The locations of Sites U1471 and U1468 have been projected northward to the east-west profile containing Sites U1465, U1466, and U1468 (Fig. 2). Not to scale; vertically exaggerated.

an exit pathway for convecting water along with venting gas. The sharp transitions in some of the pore fluid profiles are consistent with the existence of such barriers, which could reflect surfaces of subaerial exposure, marine hardgrounds, or other unconformities. These transitions often correspond to sequence boundaries identified in seismic reflection data and shipboard sedimentological analysis. For example, the rapid change in $\delta^{44/40}Ca$ values and strontium concentrations at Site U1468 occurs just above a sequence boundary at 191 mbsf, corresponding to the green line in Fig. 2 at approximately 850 ms traveltime (DS2 from Betzler et al., 2018). The sharpness of the boundary must be maintained by the lateral advection of different water masses above and below the horizon and limited diffusion or transport across the boundary. The existence of these barriers may explain the limited dispersion of the glacial water mass and the homogeneity of its geochemical properties across a depth interval hundreds of meters thick. Stratigraphic barriers to flow (or the geometry of facies associations more generally, as well as permeability anisotropy) may also shape the lateral variability and extent of the interstitial water masses. Site U1465, situated just 2 km away from Site U1466, has invariant geochemical properties down to 70 mbsf, whereas the pore fluids of all other sites, including Site U1466, begin evolving within this uppermost interval. These differences suggest the existence of a smaller advective cell that flushes young bottom waters through the uppermost Site U1465 but does not extend laterally to the east, possibly linked to the extensively lithified platform facies underneath. The glacial seawater signals at Sites U1467 and U1471, on the other hand, may be derived from westward flow originating from the eastern margin of the Maldives edifice and directed towards the center of the Inner Sea.

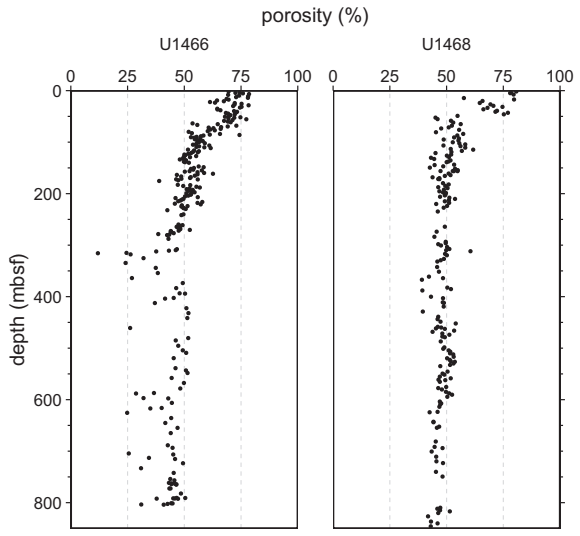

Fig. 12. Profiles of porosity at Sites U1466 and U1468, calculated from shipboard measurements of bulk and dry volume and density (Betzler et al., 2017).

4.4. Paleoceanographic and sedimentological implications

The pore fluid profiles in the Maldives reveal an archive of glacial seawater from which certain conservative properties can be simply 'read off' without the uncertainties from modeling diffusively attenuated glacial peaks. Despite this advantage over interpretations of pelagic pore fluid profiles, there are also inherent weaknesses with this approach to reconstructing features of LGM seawater. Because the water mass has penetrated the carbonate edifice 200–700 meters below the seafloor of the Inner Sea and 700–1200 meters below present sea level, none of the cores from IODP Expedition 359 can provide a record of carbonate $\delta^{18}O$ values that originated in the same water masses stored within the sediments. Since the $\delta^{18}O$ values of carbonates critically provide a temperature record (after correcting for the oxygen isotopic evolution of seawater), the Maldives pore fluid system cannot fully constrain the density of its LGM water mass as has been done for pelagic sites (Adkins et al., 2002). Additionally, the pore fluids in the Maldives represent an intermediate depth water mass that does not directly compare to the volumetrically important deep-sea glacial water masses that have been the subject of much previous work. However, this unique finding does provide new information about the paleoceanography of the glacial Indian Ocean.

The modern Indian Ocean hosts a complex pattern of surface water masses influenced by seasonal currents and monsoon precipitation, beneath which intermediate and deep water masses with origins in the Southern and Pacific Oceans as well as the Red Sea and Persian Gulf prevail (Tomczak and Godfrey, 2003; Talley, 2013). The Inner Sea of the Maldives (400–500 m depth) and the deeper flanks of the carbonate edifice are currently bathed in Circumpolar Deep Water (CDW); a tongue of relatively low salinity Antarctic Intermediate Water (AAIW) fills part of the Indian Ocean basin at intermediate depths but does not extend north of the Equator today. During the LGM, it is thought that an expanded Glacial Antarctic Intermediate Water (GAAIW) stretched further northward such that it bathed the Maldives (Jung et al., 2009). At the same time, the influence of high salinity waters from the Red Sea and Persian Gulf would have been diminished because of increased restriction and subaerial exposure from glacial sea level fall (Jung et al., 2009). From these changes in circulation, the source waters for the interstitial pore fluids of the Maldives (assumed to have penetrated the flanks of the edifice laterally) would have shifted from CDW to GAAIW during glacial times. Although this location is not directly comparable to any previous records of glacial water masses estimated from pelagic pore fluid profiles, the glacial increase in $\delta^{18}O$ values of CDW in the Southern Ocean has been estimated at 1.0–1.1‰, assuming no circulation changes at the studied sites (Malone et al., 2004).

The glacial increases in salinity and $\delta^{18}O$ values of 4.5% and 1.2‰, respectively, in the Maldives pore fluids are greater than estimated for either CDW or global mean seawater. Glacial seawater is estimated to have an average LGM salinity increase between 3.3% for a 125 m sea level drop to 3.6% for a 135 m sea level drop (Adkins et al., 2002). With the reduced importance of Red Sea and Persian Gulf waters on the glacial Indian Ocean, it is unlikely that the Maldives glacial pore fluids would be biased by this local source of high salinity, evaporated waters. As a result, the Maldives pore fluids appear to indicate that GAAIW was truly saltier than global mean seawater, although not as salty as the glacial Southern Ocean water mass with an estimated 6.6% higher salinity than the modern (an equivalent chlorinity of 596 mM) (Adkins et al., 2002). Because of the assumptions required to derive salinity estimates from diffusively attenuated pelagic pore fluid profiles, this salinity increase of 6.6% has been questioned, along with the inference that a larger distribution of salinity existed at the LGM relative to today (Miller et al., 2015; Wunsch, 2016b). The Maldives pore fluid profiles circumvent the uncertainties of the diffusive modeling and suggest at least that a more saline intermediate water mass with origins in the Southern Ocean existed during glacial times. This finding suggests that previous studies were based on decent assumptions (Adkins et al., 2002; Adkins and Schrag, 2003) and that their conclusions that salinity was a greater driver of deep-sea water mass densities than it is today are reasonable.

This system also represents a cautionary note for interpretations of sedimentary geochemistry in carbonate platforms. Based on the pore fluid data, sediments deep within the interior of the Maldives edifice are being exposed (possibly repeatedly over glacial cycles) to Pleistocene-age waters. These waters are millions of years younger than their host sediments and penetrate at least 25 km from the margin and hundreds of meters below the current depositional surface. From the behavior of reactive tracers, particularly calcium isotope ratios, the waters are also not yet fully equilibrated with the sediments across the platform system and can therefore still affect change on the bulk geochemistry of major, minor, and trace elements. In fact, sed-

imentological study of the sedimentary cores from these drill sites showed extensive diagenetic alteration of microfossils (Betzler et al., 2017). The proposed mechanism of geothermal Kohout convection in the Maldives is expected to operate in both isolated oceanic platforms as well as those on continental margins and may persist over long timescales, suggesting that many carbonate deposits may have been exposed to similar diagenetic influences. Additionally, the existence of multiple interstitial water masses of different ages and reactive histories, sometimes shaped by inferred barriers to flow with complex sedimentological and facies associations, shows how these processes can vary laterally across short (1–10 s of km) spatial scales. This variability can potentially generate a complex spatial distribution of diagenetic effects which could explain sedimentary geochemical variations on similar outcrop scales.

5. CONCLUSIONS

The composition of seawater during the Last Glacial Maximum (LGM) has so far only been estimated from indirect observations, such as through the combined use of multiple proxy measurements (e.g. $\delta^{18}O$ values in carbonates with an independent surface temperature proxy such as carbonate Mg/Ca ratios or alkenones), estimates of sea level change, or through modeling of diffusively attenuated signals in pelagic pore fluids. Through the drilling activities of IODP Expedition 359 in the Maldives, a new direct archive of a glacial water mass has been discovered within the interstitial pore fluids of carbonate sediments. A large mass of inferred LGM seawater is preserved that has likely been laterally advected through the margins of the Maldives edifice to its current position, and from which glacial chloride concentrations and $\delta^{18}O$ and δD values can be assessed. The existence of a complex structure of water masses of different ages and reactive histories is inferred from the combined observations of both conservative and reactive geochemical tracers within this system.

The discovery of this glacial water mass shapes our understanding of Indian Ocean paleoceanography, glacial thermohaline circulation more broadly, and the preservation of geochemical signals within carbonate sediments. Although similar findings are not necessarily expected to be widely replicated across different regions, the intermediate depth water mass captured at this location has substantially elevated salinity over that estimated for global mean LGM seawater, and therefore supports previous interpretations about the distribution of salinity in the glacial ocean and the assumptions made in the diffusive modeling approach to reconstructing LGM seawater. The spatial variation in water mass properties and inferred flow paths also show how variability in preservation of geochemical signals within carbonate platform sediments might arise. This system demonstrates that fluids millions of years younger than sediments can circulate on a large scale deep into the interior of a sedimentary deposit. These findings were not primary objectives of IODP Expedition 359, but rather an unexpected discovery that yielded a rich geochemical system with broad connections to glacial paleoceanography and carbonate diagenesis.

ACKNOWLEDGMENTS

This research used samples and data provided by the International Ocean Discovery Program (IODP). The authors thank the crew, technical staff, and science party of Expedition 359, with special thanks to the other shipboard geochemists, M. Inoue and M. Nakakuni. This work was supported by the IODP (PEA #AWD1004690) and the Simons Foundation (SCOL award #339006). Thanks are also due to the constructive comments from four reviewers and the associate editor that improved this manuscript.

APPENDIX A. SUPPLEMENTARY DATA

Supplementary data associated with this article can be found, in the online version, at https://doi.org/10.1016/j.gca.2019.04.030.

REFERENCES

Adkins J. F., McIntyre K. and Schrag D. P. (2002) The salinity, temperature, and $\delta^{18}O$ of the glacial deep ocean. *Science* **298**, 1769–1773.

Adkins J. F. and Schrag D. P. (2003) Reconstructing Last Glacial Maximum bottom water salinities from deep-sea sediment pore fluid profiles. *Earth Planet. Sci. Lett.* **216**, 109–123.

Aharon P., Socki R. A. and Chan L. (1987) Dolomitization of atolls by sea water convection flow: Test of a hypothesis at Niue, South Pacific. *J. Geol.* **95**, 187–203.

Aubert O. and Droxler A. W. (1996) Seismic stratigraphy and depositional signatures of the Maldive carbonate system (Indian Ocean). *Mar. Pet. Geol.* **13**, 503–536.

Betzler C., Eberli G. P., Kroon D., Wright J. D., Swart P. K., Nath B. N., Alvarez-Zarikian C. A., Alonso-García M., Bialik O. M., Blättler C. L., Guo J. A., Haffen, S ad Horozal S., Inoue M., Jovane L., Lanci L., Laya J. C., Ling Hui Mee A., Lüdmann T., Nakakuni M., Niino K., Petruny L. M., Pratiwi S. D., Reijmer J. J. G., Reolid J., Slagle A. L., Sloss C. R., Su X., Yao Z. and Young J. R. (2016) The abrupt onset of the modern South Asian Monsoon winds. *Sci. Rep.* **6**, 29838.

Betzler C., Eberli G. P., Alvarez Zarikian C. A. and the Expedition 359 Scientists (2017) Proceedings of the International Ocean Discovery Program, vol. 359. International Ocean Discovery Program, College Station, TX.

Betzler C., Eberli G. P., Lüdmann T., Reolid J., Kroon D., Reijmer J. J. G., Swart P. K., Wright J., Young J. R., Alvarez-Zarikian C., Alonso-García M., Bialik O. M., Blättler C. L., Guo J. A., Haffen S., Horozal S., Inoue M., Jovane L., Lanci L., Laya J. C., Hui Mee A. L., Nakakuni M., Nath B. N., Niino K., Petruny L. M., Pratiwi S. D., Slagle A. L., Sloss C. R., Su X. and Yao Z. (2018) Refinement of Miocene sea level and monsoon events from the sedimentary archive of the Maldives (Indian Ocean). *Prog. Earth Planet. Sci.* **5**, 5.

Betzler C., Lindhorst S., Hübscher C., Lüdmann T., Fürstenau J. and Reijmer J. (2011) Giant pockmarks in a carbonate platform (Maldives, Indian Ocean). *Mar. Geol.* **289**, 1–16.

Blättler C. L., Miller N. R. and Higgins J. A. (2015) Mg and Ca isotope signatures of authigenic dolomite in siliceous deep-sea sediments. *Earth Planet. Sci. Lett.* **419**, 32–42.

Caro G., Papanastassiou D. A. and Wasserburg G. J. (2010) ^{40}K–^{40}Ca isotopic constraints on the oceanic calcium cycle. *Earth Planet. Sci. Lett.* **296**, 124–132.

Caspard E., Rudkiewicz J.-L., Eberli G. P., Brosse E. and Renard M. (2004) Massive dolomitization of a Messinian reef in the

Great Bahama Bank: A numerical modelling evaluation of Kohout geothermal convection. *Geofluids* **4**, 40–60.

Duncan R. A. and Hargraves R. B. (1990) $^{40}Ar/^{39}Ar$ geochronology of basement rocks from the Mascarene Plateau, the Chagos Bank, and the Maldives Ridge. In *Proceedings of the Ocean Drilling Program, Scientific Results*, vol. 115, pp. 43–51. Proceedings of the Ocean Drilling Program, Scientific Results. Ocean Drilling Program, College Station, TX.

Emiliani C. (1955) Pleistocene temperatures. *J. Geol.* **63**, 538–578.

Fantle M. S. and DePaolo D. J. (2007) Ca isotopes in carbonate sediment and pore fluid from ODP Site 807A: The Ca^{2+}(aq)–calcite equilibrium fractionation factor and calcite recrystallization rates in Pleistocene sediments. *Geochim. Cosmochim. Acta* **71**, 2524–2546.

Gieskes J. M., Gamo T. and Brumsack H. (1991) *Chemical methods for interstitial water analysis aboard JOIDES Resolution*. Ocean Drilling Program, College Station, TX, USA, Technical Note 15.

Henderson G. M., Slowey N. C. and Haddad G. A. (1999) Fluid flow through carbonate platforms: Constraints from $^{234}U/^{238}U$ and Cl in Bahamas pore-waters. *Earth Planet. Sci. Lett.* **169**, 99–111.

Heuser A. and Eisenhauer A. (2008) The calcium isotope composition ($\delta^{44/40}Ca$) of NIST SRM 915b and NIST SRM 1486. *Geostand. Geoanal. Res.* **32**, 311–315.

Higgins J. A., Blättler C. L., Lundstrom E. A., Santiago-Ramos D. P., Akhtar A. A., Ahm A. S. C., Bialik O., Holmden C., Bradbury H., Murray S. T. and Swart P. K. (2018) Mineralogy, early marine diagenesis, and the chemistry of shallow-water carbonate sediments. *Geochim. Cosmochim. Acta* **220**, 512–534.

Jacobson A. D., Andrews M. G., Lehn G. O. and Holmden C. (2015) Silicate versus carbonate weathering in Iceland: New insights from Ca isotopes. *Earth Planet. Sci. Lett.* **416**, 132–142.

Jung S. J. A., Kroon D., Ganssen G., Peeters F. and Ganeshram R. (2009) Enhanced Arabian Sea intermediate water flow during glacial North Atlantic cold phases. *Earth Planet. Sci. Lett.* **280**, 220–228.

Kaufman J. (1994) Numerical models of fluid flow in carbonate platforms: Implications for dolomitization. *J. Sediment. Res.* **A64**, 128–139.

Kohout F. A. (1967) Ground-Water Flow and the Geothermal Regime of the Floridian Plateau. *Trans.—Gulf Coast Assoc. Geol. Soc.* **17**, 339–354.

Kohout F. A., Henry H. R. and Banks J. E. (1977) Hydrogeology related to geothermal conditions of the Floridan Plateau. In *The Geothermal Nature of the Floridan Plateau, Special Publication 21*. Florida Bureau of Geology.

Malone M. J., Martin J. B., Schönfeld J., Ninnemann U. S., Nürnburg D. and White T. S. (2004) The oxygen isotopic composition and temperature of Southern Ocean bottom waters during the last glacial maximum. *Earth Planet. Sci. Lett.* **222**, 275–283.

McDuff R. E. (1985) *The chemistry of interstitial waters, Deep Sea Drilling Project Leg 86. In Initial reports of the Deep Sea Drilling Project*. Government Printing Office, US, pp. 675–687.

Miller M. D., Simons M., Adkins J. F. and Minson S. E. (2015) The information content of pore fluid $\delta^{18}O$ and [Cl]. *J. Phys. Oceanogr.* **45**, 2070–2094.

Murray R. W., Miller D. J. and Kryc K. A. (2000) *Analysis of Major and Trace Elements in Rocks, Sediments, and Interstitial Waters by Inductively Coupled Plasma–Atomic Emission Spectrometry (ICP-AES)*. Ocean Drilling Program, College Station, TX, USA, Technical Note 29.

Saller A. H. (1984) Petrologic and geochemical constraints on the origin of subsurface dolomite, Enewetak Atoll: An example of dolomitization by normal seawater. *Geology* **12**, 217–220.

Sanford W. E., Whitaker F. F., Smart P. L. and Jones G. (1998) Numerical analysis of seawater circulation in carbonate platforms: I. Geothermal convection. *Am. J. Sci.* **298**, 801–828.

Schrag D. P. and DePaolo D. J. (1993) Determination of $\delta^{18}O$ of seawater in the deep ocean during the Last Glacial Maximum. *Paleoceanography* **8**, 1–6.

Schrag D. P., Hampt G. and Murray D. W. (1996) Pore fluid constraints on the temperature and oxygen isotopic composition of the glacial ocean. *Science* **272**, 1930–1932.

Schrag D. P., Adkins J. F., McIntyre K., Alexander J. L., Hodell D. A., Charles C. D. and McManus J. F. (2002) The oxygen isotopic composition of seawater during the Last Glacial Maximum. *Quatern. Sci. Rev.* **21**, 331–342.

Shackleton N. J. (1977) The oxygen isotope stratigraphic record of the Late Pleistocene. *Phil. Trans. R. Soc. Lond. B* **280**, 169–182.

Simms M. (1984) Dolomitization by groundwater-flow system in carbonate platforms. Transactions—Gulf Coast Association of Geological. *Societies* **34**, 411–420.

Talley L. D. (2013) Hydrographic Atlas of the World Ocean Circulation Experiment (WOCE). Indian Ocean, vol. 4. eScholarship, University of California.

Tomczak M. and Godfrey J. S. (2003) *Regional Oceanography: An Introduction*. .

Turchyn A. V. and DePaolo D. J. (2011) Calcium isotope evidence for suppression of carbonate dissolution in carbonate-bearing organic-rich sediments. *Geochim. Cosmochim. Acta* **75**, 7081–7098.

Whitaker F. F. and Smart P. L. (1990) Active circulation of saline ground waters in carbonate platforms: Evidence from the Great Bahama Bank. *Geology* **18**, 200–203.

Wunsch C. (2016a) Last Glacial Maximum and deglacial abyssal seawater oxygen isotopic ratios. *Clim. Past* **12**, 1281–1296.

Wunsch C. (2016b) Pore fluids and the LGM ocean salinity—reconsidered. *Quatern. Sci. Rev.* **135**, 154–170.

Yechieli Y., Yokochi R., Zilberbrand M., Lu Z.-T., Purtschert R., Sueltenfuss J., Jiang W., Zappala J., Mueller P., Bernier R., Avrahamov N., Adar E., Talhami F., Livshitz Y. and Burg A. (2019) Recent seawater intrusion into deep aquifer determined by the radioactive noble-gas isotopes ^{81}Kr and ^{39}Ar. *Earth Planet. Sci. Lett.* **507**, 21–29.

Young E. D., Galy A. and Nagahara H. (2002) Kinetic and equilibrium mass-dependent isotope fractionation laws in nature and their geochemical and cosmochemical significance. *Geochim. Cosmochim. Acta* **66**, 1095–1104.

Associate editor: Adrian Immenhauser